ISBN: 978-3-95450-232-5 ISSN: 2673-7000 doi:10.18429/JACoW-NAPAC2022-TUPA26

FRINGE FIELD MAPS FOR CARTESIAN DIPOLES WITH LONGITUDINAL AND/OR TRANSVERSE GRADIENTS*

R. Lindberg, M. Borland, ANL, Argonne, IL, USA

Abstract

Fringe field effects in dipoles can give rise to important linear and nonlinear contributions. This paper describes how to extend the classic results of Brown (SLAC Tech. Rep. SLAC-R-75) and the more recent calculations of Hwang and Lee (doi:10.1103/PhysRefSTAB.18.122401) to Cartesian dipoles with transverse and/or longitudinal gradients. We do this by 1) introducing a more general definition of the fringe field that can be applied to longitudinal gradient dipoles, 2) allowing for quadrupole and/or sextupole content in the magnet body, and 3) showing how to employ the resulting fringe maps as a symplectic transformation of the coordinates. We compare our calculation results with tracking for longitudinal and transverse gradient dipoles planned for APS-U.

THEORY

This paper describes how to extend the classic results of Brown [1] and the more recent calculations of Hwang and Lee [2] to Cartesian dipoles with transverse and/or longitudinal gradients. Cartesian dipoles have straight magnetic poles parallel to the z-axis. In this case we can write the dimensionless magnetic vector potential $a = eA/p_0$ in a gauge with vertical component $A_y = 0$ as

$$\begin{aligned} A_z &= \frac{x}{\rho}D(z) + \frac{x^3-3xy^2}{6\rho B_0}\frac{\partial^2 B_y}{\partial x^2} + \frac{x^2-y^2}{2}KQ(z) \\ &\quad - \frac{x^4-6x^2y^2-y^4}{48}KQ''(z) \end{aligned} \tag{1}$$

$$\begin{aligned} A_x &= \frac{y^2}{2\rho}D'(z) - \frac{8y^4}{192\rho}D'''(z) \\ &\quad + \frac{6x^2y^2-y^4}{24\rho B_0}\frac{\partial^2 B_y'}{\partial x^2} + \frac{xy^2}{2}KQ'(z), \end{aligned} \tag{2}$$

where the dimensionless, on-axis dipole and quadrupole field profiles are related to the generalized gradient representation [3] via

$$D(z) = \frac{q\rho}{p_0}C_1(z) \qquad Q(z) = \frac{2q}{Kp_0}C_2(z), \tag{3}$$

while the field curvature term

$$\frac{1}{\rho B_0}\frac{\partial^2 B_y}{\partial x^2} = -\frac{q}{p_0}\left[\frac{1}{4}C_1''(z) - 6C_3(z)\right]. \tag{4}$$

The hard edge model approximates the full field dependence using piece-wise constant regions. We illustrate this in Fig. 1, where we define the hard edge locations by matching the integrated bending field such that

$$\begin{aligned} &\int_{z_-}^{z_+} dz\, B_y(0,0,z) = \int_{z_-}^{z_+} dz\, C_1(z) \\ &= (z_+ - z_{\text{edge}})\Pi_1(z_+) + (z_{\text{edge}} - z_-)\Pi_1(z_-), \end{aligned} \tag{5}$$

where the step function $\Pi_1(z)$ is defined in terms of the Heaviside function as

$$\Pi_1 = C_1(z_+)\Theta(z - z_{\text{edge}}) + C_1(z_-)\Theta(z_{\text{edge}} - z). \tag{6}$$

The edge models for quadrupole and sextupole components are defined by z_{edge} and their maxima/minima at $z_\pm$, while the difference between the actual fields from Eqs. (1) and (2) and the hard edge model defines the fringe fields. The full particle motion is governed by the expanded, dimensionless Hamiltonian

$$\begin{aligned} \mathcal{H}(x,p,\delta;z) &\approx \frac{(p_x+a_x)^2\sec^3\theta}{2(1+\delta)} + \frac{p_y^2\sec\theta}{2(1+\delta)} - \delta \\ &\quad + \delta\cos\theta + (p_x+a_x)\tan\theta + a_z, \end{aligned} \tag{7}$$

while the fringe field corrections are defined by the difference of $\mathcal{H}$ and the hard edge Hamiltonian

$$\begin{aligned} \mathcal{H}_0 &= \frac{\sec^3\theta}{2(1+\delta)}p_x^2 + \frac{\sec\theta}{2(1+\delta)}p_y^2 - \delta + \delta\cos\theta \\ &\quad + p_x\tan\theta + x\frac{q}{p_0}\Pi_1(z) + (x^2-y^2)\frac{q}{p_0}\Pi_2(z) \\ &\quad + (x^3-3xy^2)\frac{q}{p_0}\Pi_3(z). \end{aligned} \tag{8}$$

Our perturbation theory proceeds by first defining $\mathscr{B}_0(z|z_-)$ to be the unperturbed map from $z_- \to z$ associated with $\mathcal{H}_0$. Then, the full map $\mathscr{M}$ for $\mathcal{H}_0 + \mathcal{H}_1$ can be written using the "reverse factorization" [4] as $\mathscr{M} = \mathscr{B}_1(z|z_-)\mathscr{B}_0(z|z_-)$, where $\mathscr{B}_1$ accounts for $\mathcal{H}_1$ such that

$$-\frac{d}{dz}\mathscr{B}_1 = \mathscr{B}_1\left(\mathscr{B}_0 :\mathcal{H}_1: \mathscr{B}_0^{-1}\right) = \mathscr{B}_1 :\mathcal{H}_1^{\text{int}}:. \tag{9}$$

We diagram these maps in Fig. 1. The fringe field map $\mathscr{F}$ obtains by sandwiching the full dipole field map $\mathscr{M}$ between unperturbed dipole maps $\mathscr{B}_0$ to and from the edge:

$$\begin{aligned} \mathscr{F} &= \mathscr{B}_0(z_-|0)\mathscr{M}\mathscr{B}_0(0|z_+) \\ &= \mathscr{B}_0(z_-|0)\mathscr{B}_1(z_+|z_-)\mathscr{B}_0(0|z_-). \end{aligned} \tag{10}$$

Finally, the fringe field map at the hard edge is written using the Magnus operator $\mathscr{F} = e^{:\Omega_M:}$ with Lie generator

$$\begin{aligned} \Omega_M &= -\int_{z_-}^{z_+} dz\, \mathcal{H}_1^{\text{int}}(z|0) \\ &\quad + \frac{1}{2}\int_{z_-}^{z_+} dz \int_{z_-}^{z} d\zeta\, :\mathcal{H}_1^{\text{int}}(\zeta|0): \mathcal{H}_1^{\text{int}}(z|0) + \ldots \end{aligned} \tag{11}$$

* Work supported by the U.S. Department of Energy, Office of Science, Office of Basic Energy Sciences, under Contract No. DE-AC02-06CH11357.

ISBN: 978-3-95450-232-5 ISSN: 2673-7000 doi:10.18429/JACoW-NAPAC2022-TUPA26

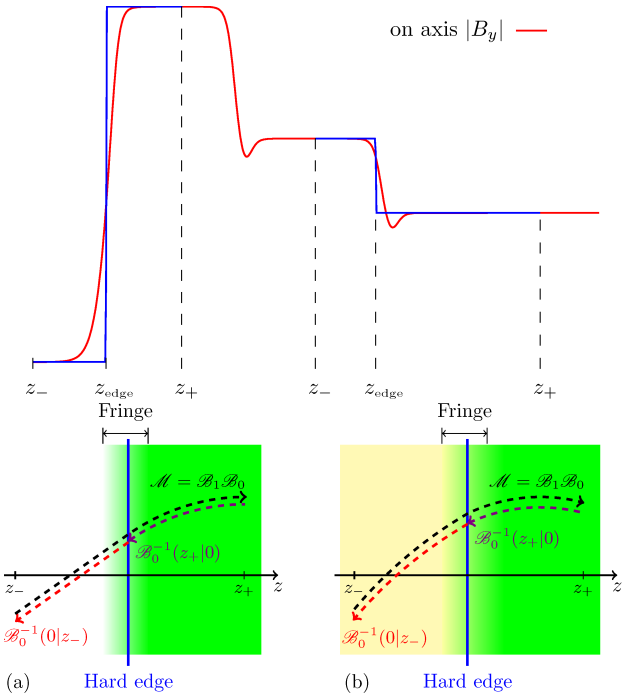

Figure 1: On the top left is the on-axis field profile (red) and hard edge model (blue) at the entrance edge where B_y starts from zero at z_- and reaches a maximum at z_+. On the top right the difference between the red and blue shows the more complicated fringe in a longitudinal gradient dipole. The bottom two panels illustrate the corresponding maps for these two cases.

The fringe field correction at the hard edge for, e.g., the vertical coordinate, is then $\Delta y = (e^{:\Omega_M:} - 1)y_0$.

The resulting fringe field maps include hard edge generalizations of [1] such as

$$\Delta x = \frac{\sec^3\theta}{2(1+\delta)}\frac{y_0^2}{\rho} \to \frac{\sec^3\theta}{2(1+\delta)}\left[\frac{y_0^2}{\rho_+} - \frac{y_0^2}{\rho_-}\right] \tag{12}$$

$$\Delta p_y = -\frac{y_0}{\rho}\left[\tan\theta + \frac{\sec^3\theta}{1+\delta}p_{x,0}\right] \to \left[\frac{y_0}{\rho_-} - \frac{y_0}{\rho_+}\right]\left[\tan\theta + \frac{\sec^3\theta}{1+\delta}p_{x,0}\right] \tag{13}$$

and new quadrupole corrections including

$$\Delta x|_{\rm new} = \frac{1 - \frac{3}{2}\tan^2\theta}{\cos^3\theta(1+\delta)}(g^2KI_1)x_0 \tag{14}$$

$$\Delta y|_{\rm new} = -\frac{\sec\theta}{1+\delta}(g^2KI_1)y_0 \tag{15}$$

$$\Delta p_x|_{\rm new} = -\frac{(1 - \frac{3}{2}\tan^2\theta)}{\cos^3\theta(1+\delta)}(g^2KI_1)p_{x,0} - \frac{\tan\theta}{4}(K_+ - K_-)(x_0^2 + y_0^2) \tag{16}$$

$$\Delta p_y|_{\rm new} = \frac{\sec\theta}{1+\delta}(g^2KI_1)p_{y,0} - \frac{\tan\theta}{2}(K_+ - K_-)x_0y_0 \tag{17}$$

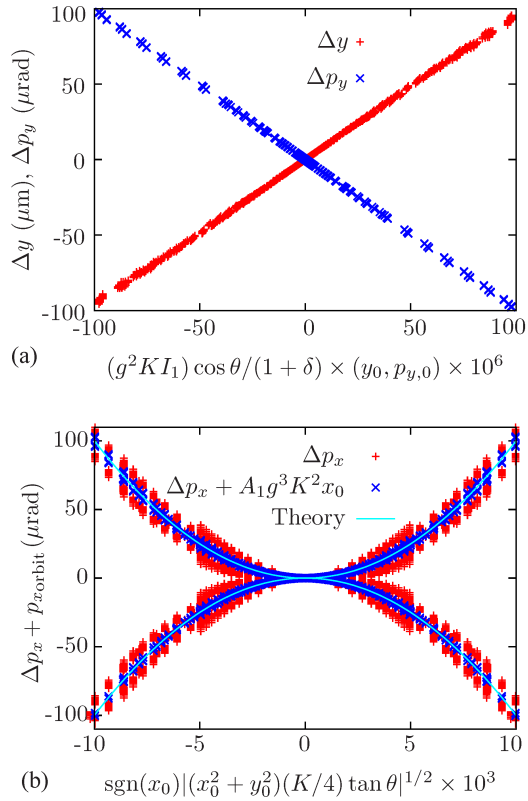

Figure 2: (a) Fringe Δy and Δp_y vs. initial y_0 and $p_{y,0}$ scaled such that Eqs. (15) and (17) predict the lines $y = \pm x$. (b) Δp_x corrected by the theory's offset $p_{x_{\rm orbit}}$ (red), and by an empirically found focusing $\propto g^3K^2x_0$. The offset is scaled so Eq. (16) follows $y = \pm x^2$ (cyan).

where g is the magnetic gap the quadrupole fringe integral

$$I_1 = \frac{2q}{g^2Kp_0}\int_{z_-}^{z_+} dz\,(z - z_{\rm edge}) \times \{C_2(z) - C_2(z_+)\Theta(z) - C_2(z_-)[1 - \Theta(z)]\}\,. \tag{18}$$

COMPARISON WITH TRACKING

Our first comparison is for an idealized fringe field, wherein we assume that the on-axis variation follows the Enge function $1/(1 + e^{-z/g})$ [5]. For this case we model the B-field using the one-parameter dipole and quadrupole solutions provided in Ref. [6], and use tracking to evaluate the fringe field map using the following four steps:

1. Initialize coordinates on the hard edge $z = z_{\rm edge} = 0$.
2. Drift particles to $z = -10g$, where $B \approx 0$.
3. Track particles through exact magnetic field to $z = 10g$, where $B \approx$ constant.
4. Back-track the particles to the hard edge $z = 0$ using the ideal $B = (p_0/q)(1/\rho + Ky, Kx, 0)$.

We summarize results of numerous tracking studies for a wide range of input coordinates, entrance angles θ, magnetic gaps g, and quadrupole strengths K in Fig. 2. Panel (a) plots the vertical magnification-like terms from Eqs. (15) and (17), where the indepedent variable was scaled such that

ISBN: 978-3-95450-232-5 ISSN: 2673-7000 doi:10.18429/JACoW-NAPAC2022-TUPA26

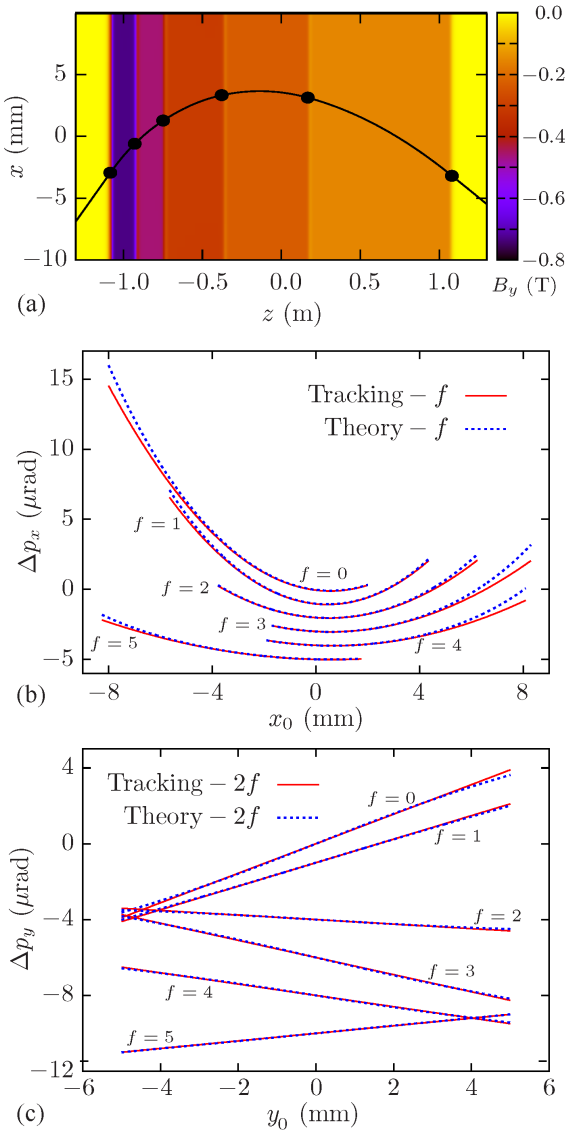

Figure 3: (a) A:M1 longitudinal gradient dipole field and reference orbit. The hard edges of each magnetic segment are marked with black circles. (b) Comparison of tracking (red solid lines) with theory (blue dashed lines) for the fringe field corrections Δp_x as a function of input x_0 at each hard edge. The lines are displaced by the fringe number $0 \le f \le 5$ for clarity. (c) Analogous comparisons of tracking and theory for the vertical focusing Δp_y at each edge.

the theory predicts lines with unit slopes. Panel (b) tests the second order corrections to p_x, where the red ones are as measured, while the blue also correct for an additional focusing term that is third-order in the gap. The theory lines are the parabolas $y = \pm x^2$.

For the next test, we consider the APS-U's A:M1 longitudinal gradient dipole [7, 8]. As shown in Fig. 3(a), the longitudinal variation is achieved by varying the field over five nearly constant steps, so that there are six hard edges as indicated by the black circles. Within each segment the hard edge model entails dipole, quadrupole, and sextupole components, while we also have six fringe field maps at each edge. We compare tracking with theory by applying the same four steps as before, but now in step 2 we track the particles using the hard edge field.

Table 1: Tune predictions for the APS-U using three different models for the Q4 reverse bend quadrupole.

Model	ν_x	ν_y
BGGEXP	94.9856	36.0878
CCBEND+Fringe	94.9832	36.0872
CCBEND+No Fringe	95.0038	36.1560

We compare the resulting predictions for the horizontal fringe maps Δp_x in Fig. 3(b). Both theory and tracking results are displaced by the fringe number f for clarity; we find that the the horizontal offset leads to both focusing and quadratic contributions. Figure 3(c) shows a similar comparison for the vertical plane. In this case we see mostly vertical focusing, which again is designed to approximately cancel any body focusing over the entire magnet.

`elegant` TRACKING

We have added the fringe field model to `elegant`'s `CCBEND` [9, 10], and then compared the resulting models against tracking in the full field. The APS-U lattice [11] uses several reverse bends [12, 13], two of which (Q4 and Q5) are straight magnets. In tests with the Q4 dipole [7], we have found that the linear matrix elements without the fringe field contributions agree to within 0.15%. Although this seems reasonably good, we have found that it is not sufficient to usefully predict the APS-U tune. Including the fringe field corrections reduces the discrepancy in linear matrix elements to the level of a few times 10^{-4}. As shown in Table 1, this leads to nearly indistinguishable results from full-field tracking.

This theory has been used in the `LGBEND` (longitudinal gradient bend) element, which models straight dipoles with an arbitrary number of segments. The fringe integrals for `CCBEND` and `LGBEND` can be easily evaluated using the companion program `straightDipoleFringeCalc`, which uses a generalized gradient expansion (GGE) to provide fields necessary to define the magnet edges and perform the fringe integrals. The GGE can be produced using two other companion programs, `computeCBGGE` and `computeRBGGE` [14], which compute the GGE from data on cylindrical or rectangular cylinders, respectively. For `LGBEND`, the `straightDipoleFringeCalc` also requires the beam trajectory, which can be provided by using the GGE with `elegant`'s `BGGEXP` element. In this case, the output is a file that provides parameters for the edges and segments, which is then loaded by the `LGBEND` element. Comparison of `LGBEND` to the much slower `BGGEXP` shows excellent agreement.

ISBN: 978-3-95450-232-5 ISSN: 2673-7000 doi:10.18429/JACoW-NAPAC2022-TUPA26

REFERENCES

[1] K. L. Brown, "A First- and Second-Order Matrix Theory for the Design of Beam Transport Systems and Charged Particle Spectrometers," Tech. Rep. SLAC-R-75, SLAC, June 1982.

[2] K. Hwang and S. Y. Lee, "Dipole fringe field thin map for compact synchrotrons," *Phys. Rev. Spec. Top. Accel. Beams*, vol. 18, 122401, 2015. doi:10.1103/PhysRevSTAB.18.122401

[3] M. Venturini, "Lie Methods, Exact Map Computation, and the Problem of Dispersion in Space Charge Dominated Beams", Ph.D. thesis, University of Maryland, MD, USA, 1998.

[4] A. J. Dragt, "Lie Methods for Nonlinear Dynamics with Applications to Accelerator Physics", University of Maryland, MD, USA, 2019.

[5] H. A. Enge, "Achromatic Magnetic Mirror for Ion Beams", *Rev. Sci. Instr.*, vol. 34, p. 385, 1963. doi:10.1063/1.1718372

[6] B. D. Muratori, J. K. Jones, and A. Wolski, "Analytical expressions for fringe fields in multipole magnets," *Phys. Rev. Accel. Beams*, vol. 18, p. 064001, 2015. doi:10.1103/PhysRevSTAB.18.064001

[7] M. S. Jaski *et al.*, "Magnet Designs for the Multi-bend Achromat Lattice at the Advanced Photon Source", in *Proc. IPAC'15*, Richmond, VA, USA, May 2015, pp. 3260–3263. doi:10.18429/JACoW-IPAC2015-WEPTY003

[8] APS-U Upgrade Project Team, "Advanced Photon Source Upgrade Project Final Design Report," Advanced Photon Source, IL, USA, Tech. Rep. APSU-2.01-RPT-003, May 2019.

[9] M. Borland, "elegant: A Flexible SDDS-Compliant Code for Accelerator Simulation," Advanced Photon Source, Chicago, IL, USA, Tech. Rep. LS-287, 2000.

[10] M. Borland, "Symplectic Integration in elegant," Advanced Photon Source, Chicago, IL, USA, Tech. Rep. LS-356, 2021.

[11] M. Borland *et al.*, "Lower Emittance Lattice for the Advanced Photon Source Upgrade Using Reverse Bending Magnets", in *Proc. NAPAC'16*, Chicago, IL, USA, Oct. 2016, pp. 877–880. doi:10.18429/JACoW-NAPAC2016-WEPOB01

[12] J. Delahaye and J. P. Potier, "Reverse Bending Magnets in Combined-Function Lattice for the CLIC Damping Ring", in *Proc. PAC'89*, Chicago, IL, USA, Mar. 1989, pp. 1611–1614.

[13] A. Streun, "The anti-bend cell for ultralow emittance storage ring lattices," *Nucl. Instrum. Methods Phys. Res., Sect. A*, vol. 737, pp. 148–154, 2014. doi:10.1016/j.nima.2013.11.064

[14] M. Borland, R. R. Lindberg, R. Soliday, and A. Xiao, "Tools for Use of Generalized Gradient Expansions in Accelerator Simulations", in *Proc. IPAC'21*, Campinas, Brazil, May 2021, pp. 253–256. doi:10.18429/JACoW-IPAC2021-MOPAB059